J. Fluid Mech. (1996), *vol.* 326, *pp.* 417–436

Eulerian and Lagrangian scaling properties of randomly advected vortex tubes

By N. A. MALIK AND J. C. VASSILICOS

Department of Applied Mathematics and Theoretical Physics, University of Cambridge, Silver Street, Cambridge CB3 9EW, UK

(Received 10 November 1994 and in revised form 24 June 1996)

We investigate the Eulerian and Lagrangian spectral scaling properties of vortex tubes, and the consistency of these properties with Tennekes' (1975) statistical advection analysis and universal equilibrium arguments. We consider three different vortex tubes with power-law wavenumber spectra: a Burgers vortex tube, an inviscid Lundgren single spiral vortex sheet, and a vortex tube solution of the Euler equation. While the Burgers vortex is a *steady* solution of the Navier–Stokes equation, the other two are *unsteady* solutions of, respectively, the Navier–Stokes and the Euler equations. In our numerical experiments we study the vortex tubes by subjecting each of them to external 'large-scale' sinusoidal advection of characteristic frequency f and length scale ρ.

Not only do we find that the Eulerian frequency spectrum $\Phi_E(\omega)$ can be derived from the wavenumber spectrum $E(k)$ using the simple Tennekes advection relation $\omega \sim k$ for all finite advection frequencies f when the vortex is steady, but also when the vortex is unsteady, and in the Lundgren case even when $f = 0$ owing to the self-advection of the Lundgren vortex by its own differential rotation.

An analytical calculation using the method of stationary phases for $f = 0$ shows that for large enough Reynolds numbers the combination of strain with differential rotation implies that $\Phi_L(\omega) \sim \omega^{-2}+\text{Const}$ for large values of ω. We verify numerically that $\Phi_L(\omega)$ does not change when $f \neq 0$. With the Burgers vortex tube we are in a position to investigate the spectral broadening of the Eulerian frequency spectrum with respect to the Lagrangian frequency spectrum. A spectral broadening does exist but is different from the spectral broadening predicted by Tennekes (1975).

1. Introduction

Twenty years ago, Tennekes wrote a paper with the title 'Eulerian and Lagrangian time microscales in isotropic turbulence'. Motivated by a discrepancy between experimentally measured Eulerian time microscales and the value predicted by Kolmogorov scaling, Tennekes (1975) advanced an advection hypothesis according to which the shape of the Eulerian high-frequency power spectrum $\Phi_E(\omega)$ is determined by large-scale advection of inertial-scale eddies. Specifically, it is assumed that random advection of inertial-scale eddies by large-scale motions is so fast that the inertial-scale eddy structure of the turbulence remains effectively 'frozen' during its passage past a fixed observation point†. Tennekes' advection hypothesis is an adaptation of Taylor's

† There are recent dynamical arguments for the validity of this assumption that are made by comparing long-range large–small-scale dynamics with local small-scale triadic dynamics through the spectral Navier–Stokes equation (see Yeung *et al.* 1995).

'frozen-turbulence' hypothesis to the advection of small inertial eddies by large-scale eddies in the turbulence.

Quantitatively, Tennekes' assumption implies a direct dependence of the Eulerian frequency spectrum $\Phi_E(\omega)$ on the wavenumber energy spectrum $E(k)$ of the turbulence. The energy $\Phi_E(\omega)\,\mathrm{d}\omega$ in the fluctuations in time seen by a fixed observer is directly proportional to the energy $E(k)\,\mathrm{d}k$ of turbulent eddies of wavenumber between k and $k+\mathrm{d}k$ provided $\omega \propto u'k$ and $\mathrm{d}\omega \propto u'\mathrm{d}k$, where u' is the r.m.s. velocity of the turbulent fluctuations. Hence, setting

$$B\omega = u'k \tag{1a}$$

where B is a constant,

$$\Phi_E(\omega) \propto u'^{-1} E\left(\frac{B\omega}{u'}\right). \tag{1b}$$

If the wavenumber spectrum $E(k)$ of the turbulence obeys Kolmogorov scaling, in which case

$$E(k) \sim \epsilon^{2/3} k^{-5/3} \tag{2}$$

where ϵ is the average rate of energy dissipation per unit mass, it then follows that

$$\Phi_E(\omega) \propto \epsilon^{2/3} u'^{2/3} \omega^{-5/3}. \tag{3}$$

Unlike the Eulerian frequency spectrum, the Lagrangian frequency spectrum $\Phi_L(\omega)$ is assumed to obey Kolmogorov scaling in the limit of high Reynolds numbers (Inoue 1951), so that, on dimensional grounds,

$$\Phi_L(\omega) \propto \epsilon\omega^{-2}. \tag{4}$$

Kolmogorov scaling also implies that (4) is valid over the inertial range of frequencies, that is for frequencies $\omega \ll \omega^L_{max}$ where

$$\omega^L_{max} \sim (\epsilon/\nu)^{1/2} \tag{5}$$

where ν is the kinematic viscosity of the fluid. Tennekes' advection hypothesis, however, implies that (3) is valid in the inertial-advective range of frequencies, that is for frequencies $\omega \ll \omega^E_{max}$ where

$$\omega^E_{max} \sim u'/\eta \tag{6}$$

and η is the Kolmogorov viscous microscale, i.e. $\eta \sim (\nu^3/\epsilon)^{1/4}$. Defining $Re_\eta = u'\eta/\nu$,

$$\frac{\omega^E_{max}}{\omega^L_{max}} \sim Re_\eta. \tag{7a}$$

Alternatively, assuming $\epsilon \sim u'^3/L$, where L is an integral length scale, and defining a Reynolds number $Re_L = u'L/\nu$,

$$\frac{\omega^E_{max}}{\omega^L_{max}} \sim Re_L^{1/4}. \tag{7b}$$

Thus, the advection hypothesis implies a broadening of the Eulerian frequency spectrum with respect to its Lagrangian counterpart. The Eulerian frequency spectrum extends to frequencies that are higher by a factor proportional to Re_η or $Re_L^{1/4}$ (figure 1).

Over the past fifteen years, direct numerical simulations (DNS) of both decaying and forced isotropic turbulence with a variety of small to moderate Reynolds numbers

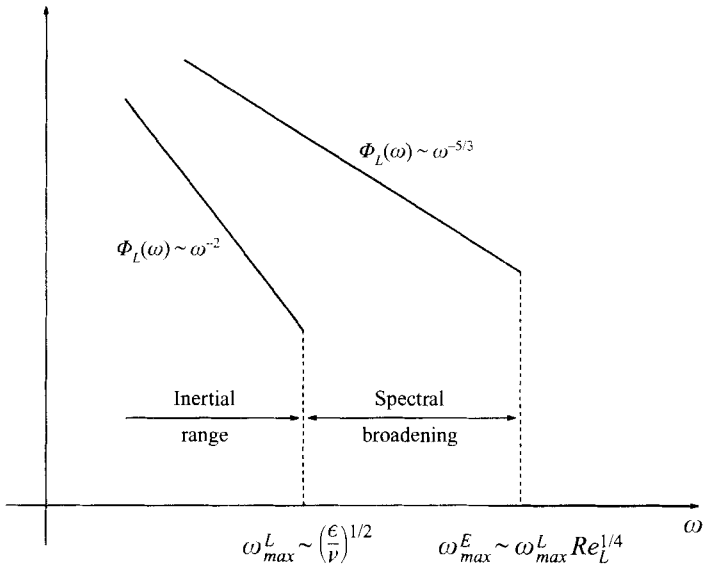

FIGURE 1. Schematic log-log plot of high-Reynolds-number Eulerian and Lagrangian turbulent frequency spectra according to Inoue (1951) and Tennekes (1975); ($\omega^E_{max} \sim Re_\eta \omega^L_{max} \sim Re_L^{1/4} \omega^L_{max}$).

Re have revealed regions of intense vorticity that are coherently organized in the form of long and slender vortex tubes (see Jiménez *et al.* 1993 and references therein). More recently, the experimental technique of migrating bubbles has been used to visualize such intense vortical filaments in shear-driven turbulence, and in homogeneous, isotropic, stationary turbulence, (see Villermaux, Sixou & Gagne 1995 and references therein). A picture, however incomplete, of the organisation of the small scales of the turbulence is emerging. At the present stage, it is not known whether this picture of small-scale turbulence where vortex tubes dominate the smallest scales survives in the limit $Re \to \infty$. Nevertheless, the purpose of this paper is to study idealized problems where the small-scale structure of the turbulence is modelled with vortex tubes that are randomly advected by a large-scale motion.

In the last decade, some progress has also been made in the understanding of the consequences of self-similar power spectra. Power spectra such as $E(k) \sim k^{-2p}$ where p is not an integer *imply* the existence of singularities that are more severe than mere discontinuities in the flow† (Hunt & Vassilicos 1991). For example, Kolmogorov's $E(k) \sim k^{-5/3}$ ($p = 5/6$) implies that high Reynolds number small-scale turbulence contains near-singularities (approximate singularities valid down to local viscous length scales where the flow is regular) that are either simple (figure 2*a*), complex isolated (figure 2*b*) or non-isolated (figure 2*c*). It has been suggested that some of the vortex tubes in the small-scale turbulence may carry some of the turbulence near-singularities (Moffatt 1984, 1993; Hunt & Vassilicos 1991) and Pullin & Saffman (1993) developed a model of the turbulence fine-scale structure based on the assumption that these vortex tubes are Lundgren vortices, which are strained rolled-up spiral vortex sheets and are an example of a flow with a *complex isolated* near-singularity. Lundgren vortices are asymptotic incompressible solutions of the Navier–Stokes equation in the limit where time $t \to \infty$. An example of an incompressible vortex tube solution of

† The converse is not necessarily true. A k^{-2p} spectrum where p is an integer can be the result of either a discontinuity in a $(p-1)$ derivative of the field or of singularities such as in figure 2.

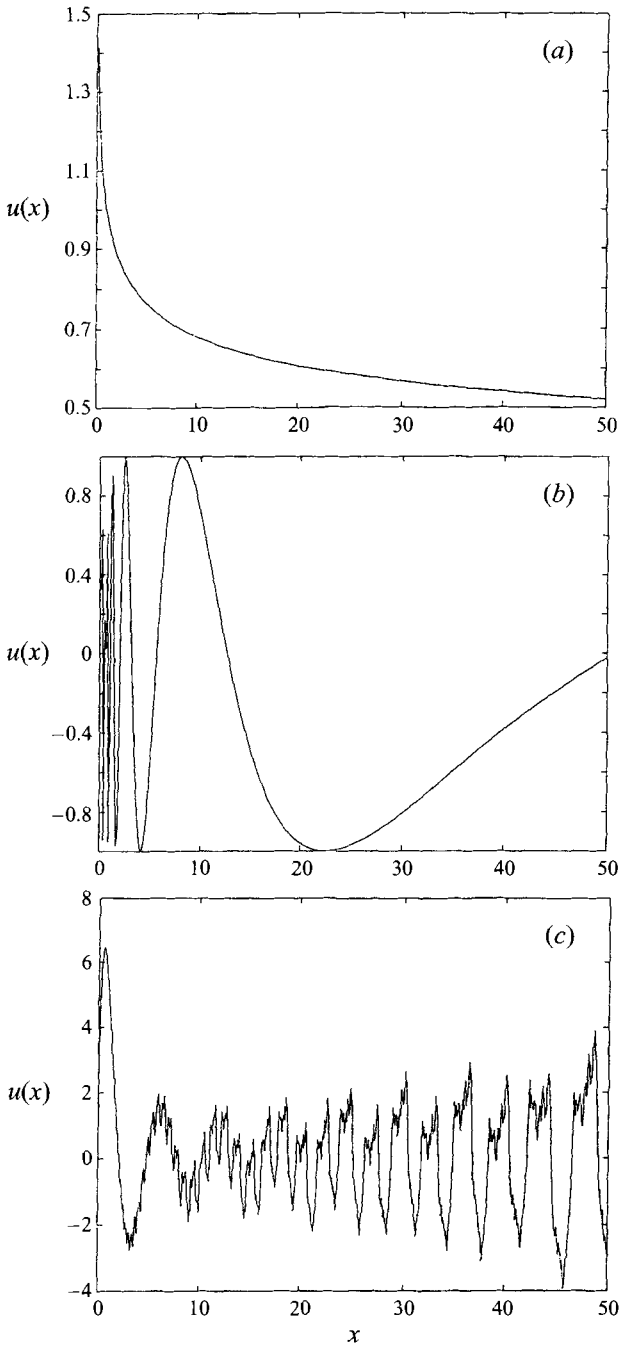

FIGURE 2. In one dimension, the following functions all have the same energy spectrum $E(k) \sim k^{-5/3}$: (*a*) $u(x) = x^{-1/6}$; (*b*) $u(x) = \sin x^{-1/2}$; (*c*) the Weierstrass function for $D = 7/6$; $u(x) = \sum_{n=0}^{\infty} k_n^{D-2} \sin(k_n x)$ where $k_n = y^n$ with $y > 1$ and $1 < D < 2$.

the Navier–Stokes equation with a *simple* near-singularity is the Burgers vortex where the azimuthal velocity $u_\phi \sim r^{-1}$ outside the viscous core, i.e. for distances r from the central axis larger than the radius of the viscous core (Batchelor 1967, pp. 271–273). Models of small-scale turbulence based on Burgers vortex tubes and vortex sheets have been discussed by Townsend (1951), and Jiménez *et al.* (1993) have assumed a Gaussian vorticity fall-off along the transversal of the vortex tube, as in the Burgers vortex. Moffatt, Kida & Okhitani (1994) explain some observed properties of DNS small-scale turbulent vortex tubes in terms of non-axisymmetric Burgers-like vortex tubes that are high-Reynolds-number asymptotic solutions of the Navier–Stokes equation.

In the range of wavenumbers where the effects of viscosity are negligible, the energy spectra of the Burgers vortex and of the Lundgren single spiral sheet vortex respectively take the forms $E(k) \sim k^{-1}$ and $E(k,t) \sim k^{-2}$ (see the Appendix). The k^{-1} spectrum of the Burgers vortex reflects the simple r^{-1} singularity of the velocity field whereas the k^{-2} spectrum of the Lundgren spiral vortex reflects the combination of a simple singularity in the differential rotation that continuously winds the vortex sheet into a spiral and of the isolated complex singularity of the spiral vorticity field. (It is by interpreting the spatial average over many spiral vortex tubes as an integration over the history of a single such vortex tube and by carrying out this integration over time that Lundgren (1982) obtains $E(k) \sim k^{-5/3}$ from $E(k,t) \sim k^{-2}$.)

In this paper, we subject each of three different vortex tubes to a sinusoidally unsteady advection, and calculate Eulerian and Lagrangian frequency spectra. The object of our investigation is to study whether and under what conditions such simple vortex models of small-scale turbulent flow structure can account for the Tennekes advection hypothesis, the spectral broadening that ensues from it, and the ω^{-2} Lagrangian spectrum that follows, in the context of the classical turbulence equilibrium theory from dimensional similarity arguments. How do the singularities of the Eulerian turbulence field affect the Eulerian and Lagrangian frequency spectra?

In the following section 2, we describe the three vortex tubes in some detail, we calculate their Eulerian frequency spectra using the Tennekes advection hypothesis and we compare these with the numerically calculated spectra. In §3 we investigate the Lagrangian frequency spectra of the three vortex tubes, and in §4 we make a few observations about the geometry of fluid element trajectories around vortex tubes. We conclude in §5.

2. Randomly advected vortices and the Tennekes advection hypothesis

2.1. *The three vortex tubes, and their wavenumber spectra*

Both the Burgers and the Lundgren vortices are strained vortex tubes with vorticity vectors all pointing in the same (the z) direction. The z-axis is the axis of the vortex tube, and in cylindrical coordinates (r, ϕ, z) the externally imposed irrotational straining velocity field has axial and radial components

$$u_z = az \tag{8a}$$

and

$$u_r = -\tfrac{1}{2}a\,r \tag{8b}$$

where a is a constant strain rate. Superimposed on this irrotational straining velocity field is, in the case of the Burgers vortex, an azimuthal velocity

$$u_\phi = \frac{\gamma}{2\pi r}(1 - \mathrm{e}^{-r^2 a/4\nu}) \tag{9}$$

where γ is the constant circulation and ν the kinematic viscosity, and in the case of the inviscid Lundgren single spiral vortex sheet, a velocity field with radial and azimuthal components

$$u_r \approx \frac{T(t)^{-2} 2\pi f(\xi)}{r\left(\dfrac{\mathrm{d}\Omega}{\mathrm{d}r}(\xi)\right)^2}[X(\xi,t)-\pi] \tag{10a}$$

and

$$u_\phi \approx 2\pi S(t) r\Omega(\xi) - \frac{2\pi f(\xi)}{T(t)\dfrac{\mathrm{d}\Omega}{\mathrm{d}r}(\xi)}[X(\xi,t)-\pi]$$

$$-\frac{2\pi T(t)^{-2}}{\dfrac{\mathrm{d}\Omega}{\mathrm{d}r}(\xi)^2}\left(\frac{\mathrm{d}f}{\mathrm{d}r}(\xi) - 2\frac{f(\xi)\dfrac{\mathrm{d}^2\Omega}{\mathrm{d}r^2}(\xi)}{\dfrac{\mathrm{d}\Omega}{\mathrm{d}r}(\xi)}\right)[\tfrac{1}{3}\pi^2 + \tfrac{1}{2}X^2(\xi,t) - \pi X(\xi,t)] \tag{10b}$$

where

$$X(\xi,t) = \phi - \Omega(\xi)T(t) - 2\pi\,\mathrm{int}\left(\frac{\phi-\Omega(\xi)T(t)}{2\pi}\right), \tag{10c}$$

the function int(x) is the integer part of x, $S(t) = \mathrm{e}^{at}$, $\xi = [S(t)]^{1/2} r$, $T(t) = \int_0^t S(\tau)\,\mathrm{d}\tau$, and

$$rf(r) = \frac{\mathrm{d}}{\mathrm{d}r}(r^2\Omega(r)) \tag{10d}$$

(see Lundgren 1982, 1993 and the Appendix). The Burgers vortex is a *steady* incompressible solution of the Navier–Stokes equation with a vorticity that has a Gaussian dependence on r,

$$\omega(r) = \frac{a\gamma}{4\pi\nu}\mathrm{e}^{-r^2/2R^2} \tag{11}$$

where R is the size of the vortex core which remains constant in time as a result of a balance between strain and viscosity and $R = (2\nu/a)^{1/2}$. The Lundgren vortex is an *unsteady* incompressible asymptotic solution of the Navier–Stokes equation for $t \to \infty$. The vorticity of an inviscid Lundgren single spiral vortex sheet is concentrated on a spiral sheet that is continuously being rolled up by a differential rotation:

$$\omega(r,\phi,t) = S(t) f(\xi)\delta[\phi - \Omega(\xi)T(t)] \tag{12}$$

where δ is the Dirac delta function, $\phi = \Omega(\xi)T(t)$ is the equation of the spiral, and $\Omega(r)$ is the angular velocity of the differential rotation.

An exact unsteady and incompressible vortex tube solution of the Euler equation is obtained by superimposing on the straining velocity field (8) an azimuthal velocity

$$u_\phi = 2\pi S(t) r\Omega([S(t)]^{1/2} r) \tag{13}$$

where $\Omega(r)$ is the angular velocity of the differential rotation. This latter velocity field is obtained by applying the Lundgren transformation (Lundgren 1982, 1993) to the velocity field $u_r = u_z = 0$, $u_\phi = 2\pi r\Omega(r)$ which is an exact incompressible steady solution of the Euler equation. The Lundgren transformation replaces r by $\xi = [S(t)]^{1/2} r$ in u_ϕ and adds the straining velocity field (8) onto the azimuthal flow thus generating the velocity field (8) and (13) which is also an exact incompressible solution of the Euler equation but is unsteady. Note that the azimuthally averaged

vorticity $(1/2\pi)\int_0^{2\pi}\omega(r,\phi,t)\,\mathrm{d}\phi$ is the same both in this exact unsteady solution of the Euler equation and in the Lundgren spiral vortex sheet (8) and (10) and is equal to $S(t)f([S(t)]^{1/2}r)$ where $f(r) = r^{-1}(\mathrm{d}/\mathrm{d}r)(r^2\Omega(r))$. Note also that the Lundgren inviscid spiral vortex sheet becomes the Euler solution (8) and (13) if the terms containing $T(t)$ and $X(\xi,t)$ in (10*a*), (10*b*) and (10*c*) are removed.

The energy spectrum† of the Burgers vortex is

$$E(k) = \gamma a k^{-1}\mathrm{e}^{-(Rk)^2}; \tag{14}$$

$E(k) \sim k^{-1}$ for $k \ll R^{-1}$ is a direct consequence of $u_\phi \approx \gamma/2\pi r$ where $r \gg R$. When $\Omega(r) = \Omega_0(r/R_0)^{-\alpha}$ where Ω_0 and R_0 are specified constants with dimensions of, respectively, a frequency and a length and α is strictly positive, the energy spectrum of the inviscid Lundgren single spiral vortex sheet takes the form

$$E(k,t) \sim k^{-2} \tag{15}$$

for any $\alpha < 3$. This k^{-2} form of the spectrum is a combined effect of the simple singularity in the azimuthally averaged vorticity $(1/2\pi)\int_0^{2\pi}\omega(r,\phi,t)\,\mathrm{d}\phi = f(r)$ and of the isolated complex singularity in the detailed spiral distribution of vorticity (see the Appendix). The azimuthally averaged vorticity $f(r)$ is related to the angular velocity $\Omega(r)$ by (10*d*), and therefore $f(r) = (2-\alpha)\Omega_0(r/R_0)^{-\alpha}$. The energy spectrum of the exact Euler solution (8) and (13) with $\Omega(r) = \Omega_0(r/R_0)^{-\alpha}$ is defined if $\frac{1}{2} < \alpha < 2$, in which case it takes the form

$$E(k,t) \sim k^{-5+2\alpha}. \tag{16}$$

Note that the energy spectra (15) and (16) are time-dependent, but that their power-law dependence on k is not time-dependent.

2.2. *Sinusoidal advection of vortex tubes and their Eulerian frequency spectra*

We simulate large-scale random advection of small-scale turbulence by assuming that the vortex tubes *and* their straining field (8) are advected together by an external one-dimentional sinusoidal flow along the $\phi = 0$ axis. Because of this flow, the displacement of the centre of the vortex from the origin of the fixed coordinate system oscillates as $\boldsymbol{r}_c(t) = (\rho\sin(ft), 0)$ in Cartesian coordinates where ρ and f are, respectively, the spatial amplitude and the frequency of the sinusoidal jitter. The r.m.s. velocity of the sinusoidal advection is

$$u' \propto \rho f. \tag{17}$$

Applying Tennekes' advection hypothesis (1) to calculate the Eulerian frequency spectra of sinusoidally advected vortices, we obtain, in the case of the Burgers vortex,

$$\Phi_E(\omega)\mathrm{d}\omega = A_E\gamma a k^{-1}\mathrm{e}^{-(Rk)^2}\mathrm{d}k \tag{18a}$$

where

$$B_E\omega = \rho f k \tag{18b}$$

and A_E and B_E are constants; in the case of the inviscid Lundgren vortex,

$$\Phi_E(\omega)\mathrm{d}\omega \sim k^{-2}\mathrm{d}k \tag{19}$$

† In principle, $\int E(k)\,\mathrm{d}k$ should be the kinetic energy per unit mass averaged over the azimuthal plane; we define $E(k)$ such that $\int E(k)\,\mathrm{d}k = 1/(4\pi(\gamma/a))\int \mathrm{d}^2\boldsymbol{x}\,\frac{1}{2}\boldsymbol{u}^2$ where γ/a is the only quantity with dimensions of an area that can be constructed independently of the viscosity ν.

where

$$\omega \sim \rho f k; \tag{20}$$

and in the case of the vortex solution (8) and (13) of the Euler equation,

$$\Phi_E(\omega)\mathrm{d}\omega \sim k^{-5+2\alpha}\mathrm{d}k \tag{21}$$

where the relation between k and ω is given by (20). From (18) it follows that the Eulerian frequency spectrum of the sinusoidally advected Burgers vortex is

$$\Phi_E(\omega) = A_E \gamma a \omega^{-1} \mathrm{e}^{-(\omega/\omega^E_{max})^2} \tag{22a}$$

where

$$\omega^E_{max} = B_E^{-1} \rho f / R, \tag{22b}$$

and from (19) and (20) it follows that the Eulerian frequency spectrum of the sinusoidally advected Lundgren single vortex sheet takes the form

$$\Phi_E(\omega) \sim \omega^{-2}, \tag{23}$$

whilst from (21) and (20) it follows that for the sinusoidally advected vortex tube Euler solution (8) and (13),

$$\Phi_E(\omega) \sim \omega^{-5+2\alpha}. \tag{24}$$

Without Tennekes' advection hypothesis, the frequency spectra of sinusoidally advected vortex tubes would have been very hard to calculate analytically. It is therefore important to verify numerically whether the Tennekes advection hypothesis leads to the right form and the right properties of the Eulerian frequency spectra of sinusoidally advected vortices. The intuitive rationale behind Tennekes' advection hypothesis is that the sinusoidal advection of vortex tubes is so fast that the vortex tubes remain effectively 'frozen' during their passage past a fixed observation point. The Burgers vortex is *steady*, and therefore remains by definition 'frozen' as it travels past an observer, which suggests that formulae (18) may be expected to apply for all values of f. However, the Lundgren vortex and the Euler solution (8) and (13) are *not* steady and Tennekes' argument would imply that (19) and (20) are not valid unless f is significantly larger than a and Ω_0, the two characteristic frequencies of the inherent unsteadiness of these two vortices. A related point is that the wavenumber spectrum $E(k,t)$ of these two vortices is time-dependent, and it is therefore highly non-trivial that the Eulerian frequency spectrum can be obtained from $E(k,t)$ by a mere application of Tennekes' advection hypothesis. On the other hand the power-law dependence of $E(k,t)$ on the wavenumber k is stationary in time.

The results of our numerical calculations show, for the sinusoidally advected Burgers and Lundgren vortices, that the Tennekes advection hypothesis gives the correct Eulerian frequency spectra $\Phi_E(\omega)$ for all finite values of f, and in the case of the Lundgren vortex, even when $f = 0$. Some results obtained for the sinusoidally advected Burgers vortex are plotted in figure 3. The characteristic frequencies of this oscillating vortex are the strain rate a and γ/ρ^2 (ρ^2/γ is the turnover time of the vortex over a length scale ρ). We calculate $\Phi_E(\omega)$ numerically for various values of the dimensionless frequencies f/a and $f\rho^2/\gamma$ in ranges where both or either are smaller or larger than 1, and find in all these ranges that formulae (22) are in good agreement with the numerical results (see figure 3). The constants A_E and B_E in (22) are universal in the limit where the vortex Reynolds number $Re_\gamma = \gamma/\nu \to \infty$ or the Reynolds number $Re_\rho = \rho^2 f/\nu \to \infty$, in the sense that these constants converge to values ($A_E \approx 0.1$ and $B_E \approx 2.0$) that are independent of ν and the other parameters of the flow.

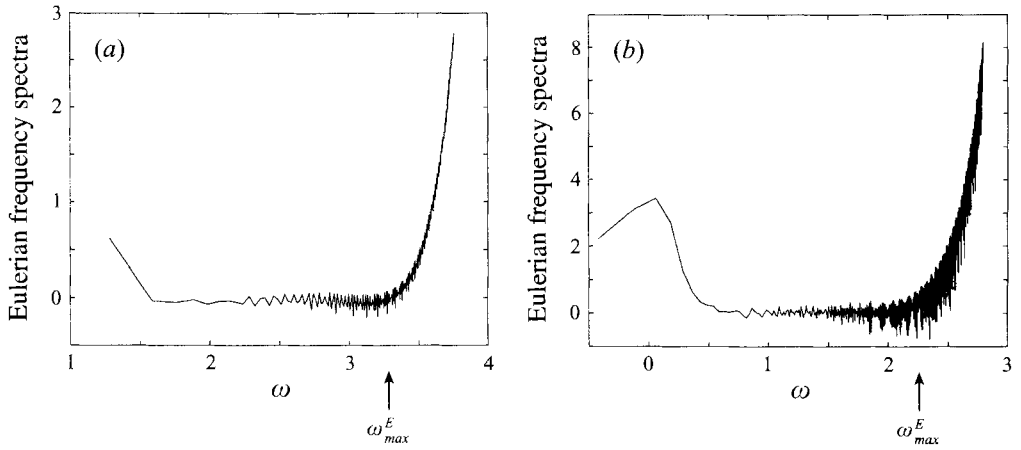

FIGURE 3. Log-log plots of the Eulerian frequency spectra against the frequency for a sinusoidally advected Burgers vortex, with advection amplitude ρ and frequency f. The ordinate is $\Phi_E(\omega)/\left(A_E(\gamma a/\omega)\exp\left(-\left(\omega/\omega^E_{max}\right)^2\right)\right)$. (*a*) $f/a = 15$, $f\rho^2/\gamma = 15$, and (*b*) $f/a = 0.05$, $f\rho^2/\gamma = 1$. a is the rate of strain, and γ is the circulation. (The Eulerian frequency spectra are obtained by averaging over an ensemble of signals observed at different points.)

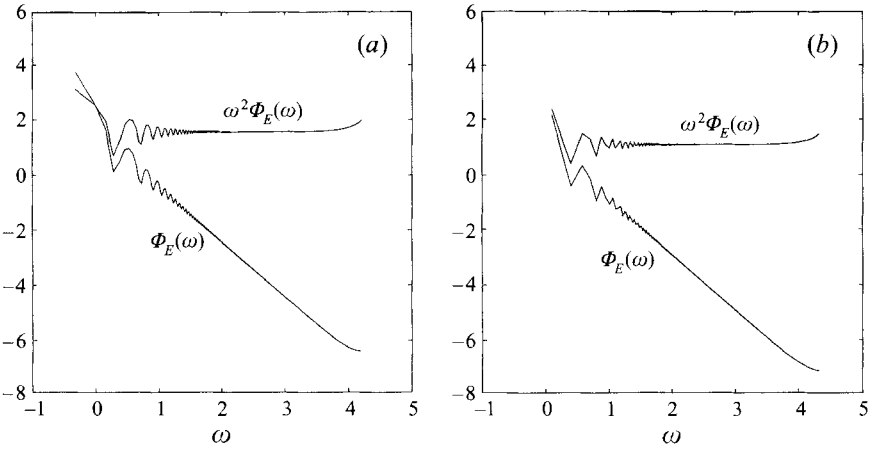

FIGURE 4. Log-log plots of the Eulerian frequency spectra against the frequency for sinusoidally advected Lundgren single spiral sheet vortex with $\alpha = 1.7$, and advection amplitude ρ and frequency f. Two graphs are shown on each plot: one shows $\Phi_E(\omega)$ and the other shows $\omega^2\Phi_E(\omega)$ to demonstrate the $\sim \omega^{-2}$ behaviour. (*a*) $f/a = 0.2$, $f/\Omega_0 = 0.2$; (*b*) $f/a = 10$, $f/\Omega_0 = 10$.

The numerically calculated Eulerian frequency spectra $\Phi_E(\omega)$ of the sinusoidally advected Lundgren single spiral vortex sheet are in good agreement with (23) for all values of the dimensionless frequencies f/a and f/Ω_0 analysed in all the ranges where these dimensionless parameters are either larger and/or smaller than 1 (figure 4). It is perhaps particularly surprising that (23) is correct even when $f = 0$ (figure 5). This result suggests that the Tennekes advection hypothesis can be valid even when the advection is a self-advection and therefore an effect of the unsteadiness of the vortex tube which does not remain frozen. In the case of the Lundgren vortex the self-advection is caused by a differential rotation whereby the spiral rotates and wraps continuously around itself into ever tighter coils.

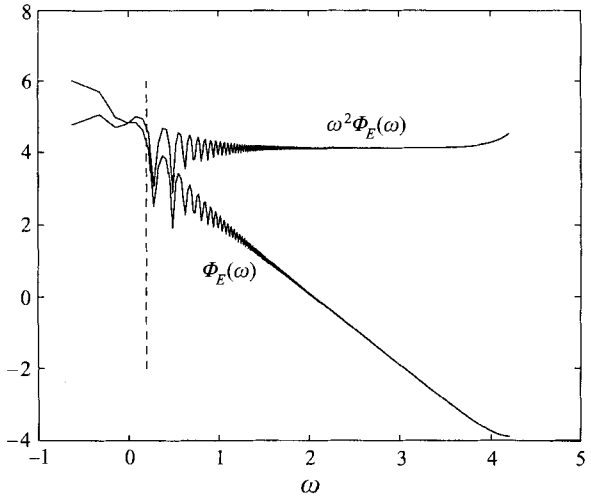

FIGURE 5. Log-log plot of the Eulerian frequency spectrum against the frequency for the Lundgren single spiral sheet vortex with $\alpha = 1.7$, with no external advection $f = 0$. Graphs for $\Phi_E(\omega)$ and for $\omega^2\Phi_E(\omega)$ are shown.

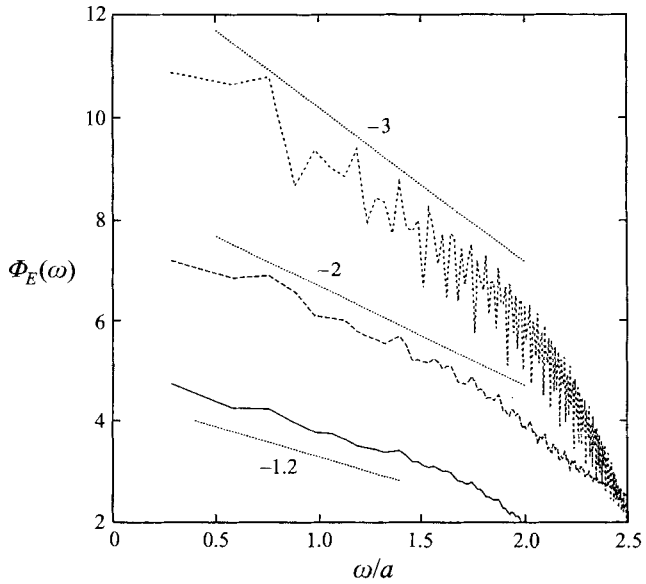

FIGURE 6. Log-log plot of the Eulerian frequency spectrum $\Phi_E(\omega)$ against the frequency for the sinusoidally advected Euler solutions (8) and (13) with $f/a = 5$, $f/\Omega_0 = 1$ and three different values of α. $\Phi_E(\omega) \sim \omega^{-3}$ for $\alpha = 1$, $\Phi_E(\omega) \sim \omega^{-2}$ for $\alpha = 1.5$ and $\Phi_E(\omega) \sim \omega^{-1.2}$ for $\alpha = 1.9$.

The Eulerian frequency spectrum of the sinusoidally advected Euler solution (8) and (13) (with $\alpha < 2$) is not defined when $f = 0$ and when $f/a \ll 1$. However, for $f/a = O(1)$ and $f/a \geqslant 1$, the numerically calculated $\Phi_E(\omega)$ is in good agreement with (24) for all values of α between $1/2$ and 2 (figure 6), and therefore the Tennekes advection hypothesis applies to the sinusoidally advected Euler solution (8) and (13) when the advection frequency f is of the same order or larger than the strain rate a.

3. Lagrangian frequency spectra

Kolmogorov scaling arguments imply that the Lagrangian frequency spectrum of the turbulence takes the form $\Phi_L(\omega) \sim \epsilon\omega^{-2}$ (Inoue 1951). It is not clear why such scaling arguments may or may not apply to the turbulence; in particular, what are the types of time and space flow structures for which Kolmogorov's dimensional arguments are valid, and under what constraints? In this section we study the form of $\Phi_L(\omega)$ that arises from a flow structure combining exponential strain and power-law differential rotation.

Let us start with the case where the vortex is not sinusoidally advected and $f = 0$. Defining the Lagrangian velocity components $u_r(t) = u_r(r(t), \phi(t), t))$ and $u_\phi(t) = u_\phi(r(t), \phi(t), t)$ where $(r(t), \phi(t))$ are cylindrical coordinates of a fluid element at time t, and defining the Fourier transformed complex Lagrangian velocity

$$\hat{u}_L(\omega) = \frac{1}{(2\pi)^{1/2}} \int \mathrm{d}t\,(u_r(t) + \mathrm{i}u_\phi(t))\mathrm{e}^{\mathrm{i}\phi(t)}\mathrm{e}^{-\mathrm{i}\omega t}, \tag{25}$$

the Lagrangian frequency spectrum is given by

$$\Phi_L(\omega) = \tfrac{1}{2}a|\hat{u}_L(\omega)|^2, \tag{26}$$

so that

$$\int \Phi_L(\omega)\,\mathrm{d}\omega = a \int \tfrac{1}{2}(u_r^2(t) + u_\phi^2(t))\,\mathrm{d}t. \tag{27}$$

The characteristic time for fluid elements to reach the vortex core is a^{-1}, and (27) is the total kinetic energy divided by this time.

We approximate the integral (25) by the method of stationary phases. The oscillation $\mathrm{e}^{\mathrm{i}(\phi(t)-\omega t)}$ is stationary at only one time $t = t_*(\omega)$ because $\phi(t)$ is a monotonically increasing function of t when $f = 0$. Assuming that $\phi(t)$ varies more rapidly with time than $u_r(t) + \mathrm{i}u_\phi(t)$ around $t = t_*$, it follows that

$$\hat{u}_L(\omega) \approx \frac{1}{(2\pi)^{1/2}}(u_r(t_*) + \mathrm{i}u_\phi(t_*))\mathrm{e}^{\mathrm{i}(\phi(t_*)-\omega t_*)} \int \mathrm{d}t\,\mathrm{e}^{\mathrm{i}\phi''(t_*)(t-t_*)^2/2} \tag{28}$$

where $\phi'' = \mathrm{d}^2\phi/\mathrm{d}t^2$, and therefore

$$\Phi_L(\omega) \approx \frac{a}{\phi''(t_*)}[u_r^2(t_*) + u_\phi^2(t_*)] \tag{29}$$

for large frequencies ω. If the time $t_*(\omega)$ is smaller than the time t_v that it takes a fluid element starting at r_0 to reach the viscous core, then $t_*(\omega)$ and the spectrum (29) may be calculated by taking into account only the velocity field *outside* the viscous core. For the Burgers vortex, the time t_v is given by $R = r_0\mathrm{e}^{-at_v/2}$ which implies $t_v = a^{-1}\ln(r_0^2 a/2\nu)$. The inviscid Lundgren vortex and the Euler solution (8) and (13) have, by definition, no viscous core and $t_v = \infty$.

3.1. *The Burgers vortex*

When $f = 0$, the coordinates $(r(t), \phi(t))$ of fluid element trajectories in the Burgers vortex *outside* the vortex core are solutions of the strain equation

$$\frac{\mathrm{d}r}{\mathrm{d}t} = u_r = -\tfrac{1}{2}ar \tag{30a}$$

and the point vortex equation

$$\frac{\mathrm{d}\phi}{\mathrm{d}t} = \frac{1}{r}u_\phi \approx \frac{\gamma}{2\pi r^2}, \tag{30b}$$

and are given by

$$r(t) = r_0 e^{-at/2} \tag{31a}$$

and

$$\phi(t) = \phi_0 + \Phi(e^{at} - 1) \tag{31b}$$

where (r_0, ϕ_0) are initial coordinates and $\Phi = \gamma/2\pi r_0^2 a$. It follows that $u_r(t) = -\frac{1}{2}a r_0 e^{-at/2}$, $u_\phi(t) \approx \gamma/2\pi r_0 e^{at/2}$, and that the projected trajectories on the azimuthal plane outside the viscous core take the spiral form $\phi(t) \sim r(t)^{-2}$. This specific spiral form is a consequence of the combination of a point vortex with the straining field (8). We shall now see that the combination of strain with the differential rotation of a point vortex implies that the Lagrangian frequency spectrum of the vortex takes the form $\Phi_L(\omega) \approx \gamma/2\pi[(2\omega/a)^{-2} + 1]$ in a range of frequencies ω such that $2\pi a \ll \omega < (Re_\gamma/4\pi)a$ when Re_γ is large enough.

If we neglect the velocity field inside the viscous core, the time t_* when the oscillation $e^{i(\phi(t)-\omega t)}$ is stationary may be calculated using (31b). We find

$$t_* = a^{-1} \ln\left(\frac{\omega}{\Phi a}\right), \tag{32}$$

and t_* cannot be defined unless $\omega > \Phi a$, which is satisfied if we take the initial distances r_0 to be large enough because $\Phi = \gamma/2\pi r_0^2 a$. We can use (29) to estimate $\Phi_L(\omega)$ if $\phi(t)$ varies more rapidly with time than $u_r(t) + iu_\phi(t)$ around $t = t_*$, and we can substitute t_* by (32) in (29) only if $t_*(\omega) < t_\nu$. Based on (30) and (31), the condition for $\phi(t)$ to vary more rapidly with time than $u_r(t) + iu_\phi(t)$ around $t = t_*$ is $2\pi a \ll \omega$, in which case (29) can be used and implies

$$\Phi_L(\omega) \approx \omega^{-1}[u_r^2(t_*) + u_\phi^2(t_*)] \tag{33}$$

which, however, is not valid in the range of large frequencies ω where $t_*(\omega) > t_\nu$ and where the viscosity affects the Lagrangian frequency spectrum. Inserting the forms of the point vortex and the straining field that make the Burgers vortex, the Lagrangian frequency spectrum (33) becomes

$$\Phi_L(\omega) \approx \frac{\gamma}{2\pi}\left[\left(\frac{2\omega}{a}\right)^{-2} + 1\right], \tag{34}$$

and is valid if $\Phi a = \gamma/2\pi r_0^2 < \omega$, $2\pi a \ll \omega$ and $\omega < (Re_\gamma/4\pi)a$ where $t_*(\omega) < t_\nu$. Such a range of frequencies exists provided that $Re_\gamma \gg 8\pi^2$ and r_0 is large enough (in particular, $r_0 > R$.) The validity of (34) is corroborated by numerical integration of Lagrangian fluid element trajectories around a Burgers vortex tube (figure 7).

We stress that the Lagrangian frequency spectrum (34) is independent of the viscosity ν because this spectrum is the signature of the combination of strain and differential rotation *outside* the viscous core of the vortex. The Kolmogorov scaling argument leading to $\Phi_L(\omega) \sim \epsilon\omega^{-2}$ in small-scale turbulence is based on the assumption that both the form of the spectrum and ϵ are independent of ν in the limit of indefinitely high Reynolds numbers. The energy dissipation rate of the velocity field ($u_z = az$, $u_r = -\frac{1}{2}ar$, $u_\phi = u_\phi(r)$) is $\nu(\frac{3}{2}a^2 + ((\partial/\partial r)u_\phi - \frac{1}{2}\omega)^2)$. Whereas the external strain rate is a, the vortex-induced strain rate is $(\partial/\partial r)u_\phi - \frac{1}{2}\omega$, and correspondingly, the external dissipation rate is $\nu\frac{3}{2}a^2$ and the vortex-induced dissipation rate is $\nu((\partial/\partial r)u_\phi - \frac{1}{2}\omega)^2$. Defining $\epsilon(r) = \nu((\partial/\partial r)u_\phi - \frac{1}{2}\omega)^2$ in the context of the Burgers vortex, it follows from (9) and (11) that $\epsilon(r) = \epsilon_0(Re_\gamma/4\pi)[e^{-2r^2/R^2} - \frac{2R^2}{r^2}(1 - e^{-2r^2/R^2})]$ with $\epsilon_0 = \gamma a^2/16\pi$. It is interesting to note that $2\pi\int_0^\infty \epsilon(r) r\,dr$ is

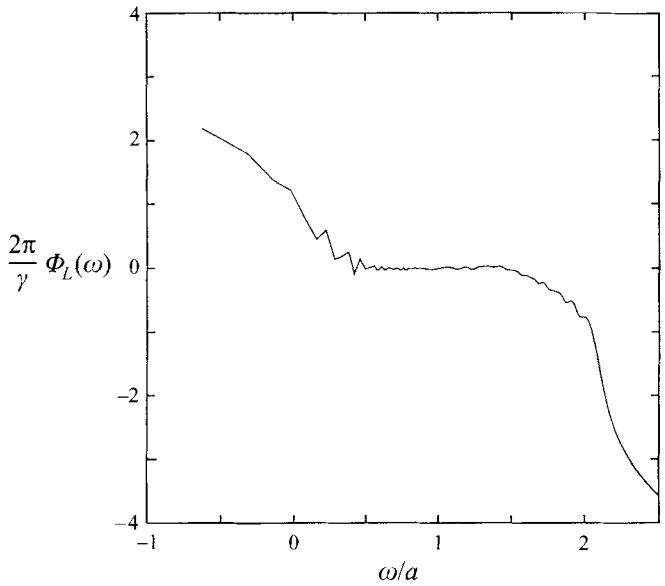

FIGURE 7. Log-log plot of the normalized Lagrangian frequency spectrum $(2\pi/\gamma)\Phi_L(\omega)$ against the normalized frequency ω/a for the Burgers vortex ($f = 0$). (The Lagrangian frequency spectra are obtained by averaging the spectra of signals observed along different fluid trajectories, each with a different starting position.)

independent of ν and proportional to ϵ_0, and that the Lagrangian frequency spectrum of the Burgers vortex is $\Phi_L(\omega) \approx 2\epsilon_0\omega^{-2}+\gamma/2\pi$ in the limit of high Reynolds numbers $\frac{Re_\gamma}{8\pi^2} \gg 1$ and in a range of frequencies that is bounded from above by

$$\omega^L_{max} = \frac{Re_\gamma}{4\pi}a. \tag{35}$$

3.2. *The exact vortex solution of the Euler equation*

The trajectories of fluid elements in the inviscid vortex Euler solution (8) and (13) are solutions of the strain equation

$$\frac{\mathrm{d}r}{\mathrm{d}t} = u_r \approx -\tfrac{1}{2}a\,r \tag{36a}$$

and of the strained differential rotation equation

$$\frac{\mathrm{d}\phi}{\mathrm{d}t} = \frac{1}{r}u_\phi \approx 2\pi S(t)\Omega([S(t)]^{1/2}r) = 2\pi S(t)\Omega_0[[S(t)]^{1/2}r/R_0]^{-\alpha}. \tag{36b}$$

It is perhaps interesting that the solutions of equations (36) take the form (31) albeit with $\Phi = 2\pi\Omega_0/a(r_0/R_0)^{-\alpha}$ and are therefore identical to the fluid element trajectories in a Burgers vortex outside the viscous core. In particular, the time-dependence of $u_r(t)$ and $u_\phi(t)$ is identical to that in the Burgers vortex and the spiral form of the projection of these trajectories on the azimuthal plane is again $\phi(t) \sim r(t)^{-2}$. In the previous subsection we have shown how trajectories of the form (31) around a Burgers vortex imply that $\Phi_L(\omega)$ is given by (34) for large Re_γ and r_0 and in a range

of frequencies $\omega \gg 2\pi a$; in the present case the same trajectories imply

$$\Phi_L(\omega) \approx 2\pi\Omega_0 R_0^{\alpha} r_0^{2-\alpha} \left[\left(\frac{2\omega}{a} \right)^{-2} + 1 \right] \tag{37}$$

under the conditions that $2\pi\Omega_0(r_0/R_0)^{-\alpha} < \omega$ for the time t_* defined in (32) to exist and $2\pi a \ll \omega$ for the stationary phase asymptotic to be valid. There is no upper bound on the frequencies ω over which the form (37) of the spectrum extends because $t_v = \infty$ in the Euler solution (8) and (13).

It is worth stressing that, similarly to the Burgers vortex, the combination of strain and differential rotation implies an ω^{-2} + Const. Lagrangian energy spectrum for $\omega \gg 2\pi a$ and r_0 large enough. Numerical integrations of fluid element trajectories around vortex Euler solutions of the form (8) and (13) corroborate the result (37) and the numerically calculated Lagrangian frequency spectra are very similar to those in figure 7 albeit with a normalization in agreement with (37).

3.3. *The Lundgren vortex*

Our numerical results for the Lagrangian frequency spectrum of the Lundgren vortex are in good agreement with a constant high-frequency spectrum, but we have no evidence of a ω^{-2} spectrum at lower frequencies. Thus, the high-frequency end of $\Phi_L(\omega)$ of the Lundgren vortex has a similar constant appearance to the $\Phi_L(\omega)$ of the Burgers vortex, even though the latter is dominated by the overall differential rotation and strain of the flow, and not by the discontinuities in the Lagrangian velocity, caused by the spiral vortex sheet, that appear in the Lundgren vortex flow. Because of these discontinuities across the vortex sheet, the stationary phase analysis leading to (29), (34) and (37) cannot be applied to the Lundgren vortex, and it is therefore quite surprising that the high-frequency Lagrangian spectrum of this vortex is constant. As for the lower frequencies, we have neither analytical nor numerical evidence pointing to a range of frequencies where the Lundgren spiral vortex sheet has a ω^{-2} Lagrangian frequency spectrum. Some of the numerical evidence we report in §4 demonstrates that the spiral form of fluid element trajectories in the Lundgren single spiral vortex sheet is *not* $\phi(t) \sim r(t)^{-2}$, contrary to the prediction of equations (31) which are valid for both the Burgers vortex and the Euler solution (8) and (13) and which lead to the Lagrangian spectra (34) and (37). Hence, the vortex sheet cannot be neglected when we calculate Lagrangian trajectories and frequency spectra. The effect of spiral vortex sheets on Lagrangian frequency spectra lies beyond the scope of the present paper and is left for subsequent study.

3.4. *The case of non-vanishing advection frequencies f*

We now integrate trajectories of fluid elements in a sinusoidally advected vortex and compute the Lagrangian frequency spectrum $\Phi_L(\omega)$. The centre $\boldsymbol{r}_c(t)$ of the vortex is given by $\boldsymbol{r}_c(t) = (\rho\sin(ft), 0, 0)$ in Cartesian coordinates and is therefore such that

$$\frac{\mathrm{d}}{\mathrm{d}t}\boldsymbol{r}_c(t) = \boldsymbol{u}_c(t) = (\rho f\cos(ft), 0, 0). \tag{38}$$

The Lagrangian velocity $\mathbf{u}(t)$ of a fluid element in the sinusoidally advected vortex is

$$\boldsymbol{u}(t) = \boldsymbol{u}_c(t) + u_z(z(t))\boldsymbol{e}_z + u_r(r'(t), \phi'(t), t)\boldsymbol{e}_{r'} + u_\phi(r'(t), \phi'(t), t)\boldsymbol{e}_{\phi'} \tag{39}$$

where $(r'(t), \phi'(t), z(t))$ are the cylindrical coordinates of $\boldsymbol{r}' = \boldsymbol{r}(t) - \boldsymbol{r}_c(t)$ where $\boldsymbol{r}(t)$ is the position of the fluid element at time t, $\boldsymbol{e}_z$ is the unit vector on the z-axis,

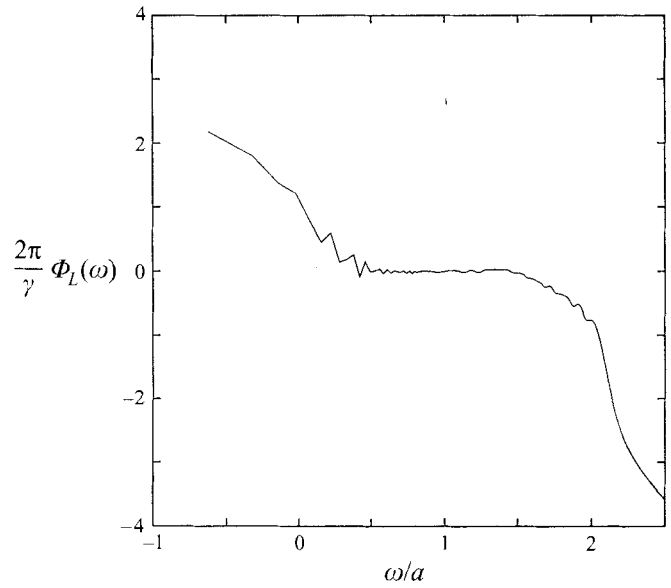

FIGURE 8. Log-log plot of the Lagrangian frequency spectrum $(2\pi/\gamma)\Phi_L(\omega)$ against the normalized frequency ω/a for the sinusoidally advected Burgers vortex for $f/a = 5$ and $f\rho^2/\gamma = 125$. This result is identical to figure 7.

$\boldsymbol{e}_{r'} = (1/r'(t))\boldsymbol{r}'$, and $\boldsymbol{e}_{\phi'}$ is defined such that $\boldsymbol{e}_{\phi'}\cdot\boldsymbol{e}_{r'} = 0$ and $\boldsymbol{e}_{r'} \times \boldsymbol{e}_{\phi'} = \boldsymbol{e}_z$. Fluid element trajectories are obtained by solving

$$\frac{\mathrm{d}}{\mathrm{d}t}\boldsymbol{r}(t) = \boldsymbol{u}(t). \tag{40}$$

The vortex tubes and the fluid elements are advected together by the same sinusoidal velocity field $\boldsymbol{u}_c(t)$ which is independent of position. Thus the motion of the fluid elements *with respect to the vortex centre* is due to the vortex tube alone and is therefore *independent of large-scale advection.* We may therefore expect the Lagrangian frequency spectra $\Phi_L(\omega)$ of sinusoidally advected vortex tubes to be identical to the Lagrangian frequency spectra of these vortex tubes when $f = 0$. This conclusion is valid for all frequencies f and is confirmed numerically for all three vortex tubes. In figure 8 we present an example of a log-log plot of $\Phi_L(\omega)$ against ω/a for the Burgers vortex when $f/a \gg 1$. Figure 8 does not differ from figure 7 where $f = 0$.

3.5. *Spectral broadening*

In the case of the sinusoidally advected Burgers vortex we have seen that $\omega^E_{max} \propto u'/R$ with $u' \propto \rho f$ and $\omega^L_{max} \propto Re_\gamma a \propto Re_\gamma \nu/R^2$. The microscale R defined under equation (11) is the viscous length scale of the vortex and is analogous to the Kolmogorov microscale η. Hence, in this model of a randomly advected strained vortex, $Re_\eta = u'R/\nu$, and

$$\frac{\omega^E_{max}}{\omega^L_{max}} \sim Re_\eta/Re_\gamma \tag{41a}$$

which is different from the spectral broadening (7*a*) predicted by Tennekes (1975) on the basis of his advection hypothesis and Inoue's (1951) Kolmogorov scaling arguments. However, the dependencies of $\omega^E_{max}/\omega^L_{max}$ on u' and R in (41*a*) are identical to those of Tennekes (1975). Assuming, following Kolmogorov, that the

average rate of energy dissipation per unit mass is set by the large-scale motions and therefore scales as $\epsilon \sim u'^3/\rho \propto \rho^2 f^3$ and equating it to the external dissipation rate which scales as νa^2 we get a relation between the strain rate a, the viscosity ν and the parameters ρ and f of the random advection that implies

$$\frac{\omega^E_{max}}{\omega^L_{max}} \sim Re_\rho^{1/4}/Re_\gamma \tag{41b}$$

where $Re_\rho = u'\rho/\nu \sim \rho^2 f/\nu$. Identifying the length scale ρ with an integral length scale of the turbulence L, (41b) is different from Tennekes' spectral broadening result (7b). Nevertheless, it is worth noting that the dependencies of $\omega^E_{max}/\omega^L_{max}$ on the large-scale quantities u', ρ and f in (41b) are identical to those predicted by Tennekes (1975) in his formula (7b).

4. Kolmogorov capacity of fluid element trajectories around vortex tubes

Because the external jitter advects the vortex and the fluid elements together without displacing them relative to each other, the shape of the Lagrangian frequency spectrum $\Phi_L(\omega)$ does not depend on f and we find by solving (38), (39) and (40) numerically that fluid element trajectories $\boldsymbol{r}(t)$ are always spiral-helical in nature and also independent of the value of f.

In the terminology of Vassilicos & Hunt (1991), the spiral trajectories sample the field by being more or less *locally* space-filling – 'locally' meaning around only the central axis of the flow – and this allows their degree of 'space-fillingness' to be measured with Kolmogorov capacities. We measure numerically the Kolmogorov capacity D_K^L of fluid element trajectories generated by the sinusoidally advected vortex tubes. In the case of the Burgers vortex we find that D_K^L is well-defined and equal to D_K^E, the Kolmogorov capacity of streamlines. For the Burgers vortex, $D_K^E = 4/3$ (Vassilicos & Brasseur 1996). On the other hand, in the range of parameters that we have investigated in this paper for the inviscid Lundgren single spiral vortex sheet, we find that $D_K^L = 5/4$ both for $f = 0$ and $f \neq 0$ and does not vary with the exponent α that characterizes the differential rotation nor with f (figures 9). This result demonstrates that the projection of fluid element trajectories on the azimuthal plane does not take the spiral form $\phi(t) \sim r(t)^{-2}$ which would have implied $D_K^L = 4/3$ (see Vassilicos & Hunt 1991). In particular, when $f = 0$, it follows that the fluid element trajectories of the inviscid Lundgren spiral vortex sheet are not well represented by the solutions of the system of equations (36). This system of equations would be derived for the inviscid Lundgren spiral vortex if the contribution of the spiral vortex sheet in (10) could be neglected. Hence, however small the amplitude of the velocity field induced by the spiral vortex sheet, the effects of the spiral vortex sheet on fluid element trajectories, and therefore also on Lagrangian frequency spectra, cannot be overlooked.

5. Discussion

Recent experimental results and direct numerical simulations of turbulence have shown that the fine scales of a turbulent flow contain long and slender vortex tubes. We confirm the validity of the Tennekes advection hypothesis for a randomly advected Burgers vortex which is a steady solution of the Navier–Stokes equation with a simple singularity that gives rise to a k^{-1} wavenumber spectrum. We also confirm the validity of the Tennekes advection hypothesis for a randomly advected unsteady vortex tube

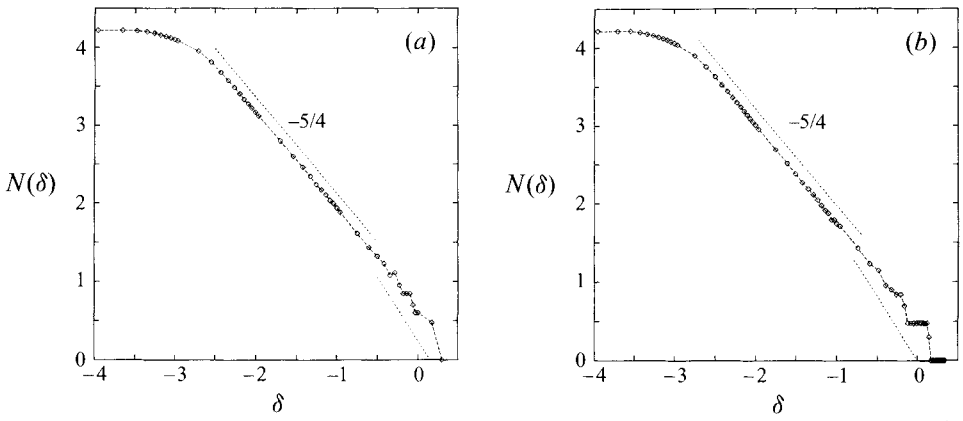

FIGURE 9. Kolmogorov capacities of fluid element trajectories in a Lundgren single spiral sheet vortex. Log-log plots of $N(\delta)$, the number of boxes that cover the trajectory, against δ, the box size; the Kolmogorov capacity D_K^L is given by $N(\delta) \sim \delta^{-D_K^L}$ if such a power law exists. (*a*) $\alpha = 1.7$, $f/a = 0.1$, $f/\Omega_0 = 2$. (*b*) $\alpha = 1.9$, $f = 0$.

solution of the Euler equation. This Euler solution has a simple singularity that gives rise to a power-law wavenumber spectrum between k^{-1} and k^{-4} ($E(k) \sim k^{-5+2\alpha}$ for $\frac{1}{2} < \alpha < 2$.) The Tennekes advection hypothesis also holds for the randomly advected Lundgren single spiral vortex sheet which is an unsteady approximate solution of the Navier–Stokes equation with an isolated complex singularity that gives rise to a k^{-2} wavenumber spectrum. But in this case we have discovered a new régime where the Eulerian frequency spectrum is still obtainable from Tennekes' relation $\omega \sim k$ even when the advection of the Lundgren vortex is purely self-induced by the inherent unsteadiness of the vortex itself with no external advection. The Eulerian frequency spectrum reflects the self-similarity of the vortex singularity in the inertial-advective range of frequencies $\omega \ll \omega_{max}^E$.

It is perhaps striking that the two different systems of equations (30) for the Burgers vortex, and (36) for the Euler solution (8) and (13), have identical solutions given by (31) in spite of the qualitative differences between (30) and (36). The system of equations (30) is a combination of strain with the steady differential rotation of a point vortex, whereas the system of equations (36) is a combination of strain with unsteady differential rotation of spatial scaling exponent α. The solutions are fluid element trajectories with projections on the azimuthal plane that take the same spiral form $\phi \sim r^{-2}$ regardless of the value of α. The combination of strain with differential rotation expressed in the solution's form (31) implies, analytically, that $\Phi_L \sim \omega^{-2} + \text{Const.}$ where $\omega \gg 2\pi a$ provided the vortex Reynolds number Re_γ is large enough or infinite. However, the presence of the spiral vortex sheet in the Lundgren vortex influences the spiral form of the fluid element trajectories to the point that these trajectories are not such that $\phi \sim r^{-2}$ and therefore do not obey (31). Nevertheless, $\Phi_L \sim \text{Const.}$ where $\omega \gg \frac{1}{2}a$ even for the Lundgren single spiral vortex sheet when $f = 0$.

When the vortex and the fluid elements are advected together by an external jitter, then for any finite advection frequency $f > 0$, $\Phi_L(\omega)$ is identical to the case when $f = 0$. When $f = 0$ and in the case of the Burgers vortex, the combined strain and differential rotation of the vortex imply that

$$\Phi_L(\omega) \approx 2\epsilon_0 \omega^{-2} + \frac{\gamma}{2\pi} \tag{42}$$

in the limit of high Reynolds number Re_γ and in a range of frequencies where $\omega \ll \omega^L_{max} \propto aRe_\gamma$. ϵ_0 is a characteristic vortex-induced energy dissipation rate per unit mass, and the first term of the right-hand side of (42) is similar to the Lagrangian energy spectrum of the turbulence obtained by Inoue (1951) by universality scaling arguments à la Kolmogorov. However, this $\epsilon_0\omega^{-2}$ term is overshadowed by the constant $\gamma/2\pi$ in (42). Furthermore, in this regime of low frequencies f, there is a spectral broadening of the Eulerian spectrum with respect to the Lagrangian spectrum that is different from, though in some ways comparable to the spectral broadening discussed by Tennekes (1975). Indeed, for the Burgers vortex where we keep the effects of viscosity, $\omega^E_{max}/\omega^L_{max} \sim Re_\eta/Re_\gamma$ to be contrasted with Tennekes' relation $\omega^E_{max}/\omega^L_{max} \sim Re_\eta$. Assuming, following Tennekes (1975), that $\epsilon \sim u'^3/\rho \propto \rho^2 f^3$ and equating ϵ to the external dissipation rate va^2, we get $\omega^E_{max}/\omega^L_{max} \sim Re_\rho^{1/4}/Re_\gamma$ which differs from Tennekes' spectral broadening relation $\omega^E_{max}/\omega^L_{max} \sim Re_\rho^{1/4}$. However, these two different spectral broadening relations bear the same dependencies on the external large-scale quantities u', ρ and f.

We are grateful to James G. Brasseur and one anonymous referee for their perceptive comments and valuable suggestions. J.C.V. acknowledges financial support from the European Community under contract No. CHRX-CT92-00091 and from the Royal Society. N.A.M. acknowledges financial support from the European Community under research contract No. ERBCHBI-CT94-1230. Part of the computational resources for this work was made available from the Institut du Developement et des Resources en Informatique Scientifique (IDRIS), which receives major funding from the Centre National de la Recherche Scientifique (CNRS).

Appendix. The Lundgren single spiral vortex sheet and its energy spectrum

The radial and azimuthal components of the velocity field around the Lundgren single spiral vortex sheet are given by

$$u_r = -\frac{ar}{2} + \frac{1}{2}\frac{\partial}{\partial\phi}\Psi([S(t)]^{1/2}r, \phi, T(t)), \tag{A1a}$$

$$u_\phi = -\frac{\partial}{\partial r}\Psi([S(t)]^{1/2}r, \phi, T(t)), \tag{A1b}$$

where, as $t \to \infty$,

$$\frac{1}{2\pi}\Psi(r,\phi,t) = \frac{1}{2\pi}\Psi_0(r) + \frac{t^{-2}f(r)}{(\frac{\mathrm{d}\Omega(r)}{\mathrm{d}r})^2}\left(\frac{\pi^2}{3} + \frac{1}{2}\left[\phi - \Omega(r)t - 2\pi\mathrm{int}\left(\frac{\phi-\Omega(r)t}{2\pi}\right)\right]^2 - \pi\left[\phi - \Omega(r)t - 2\pi\mathrm{int}\left(\frac{\phi-\Omega(r)t}{2\pi}\right)\right]\right) + O(t^{-3}) \tag{A2a}$$

and

$$\frac{\partial}{\partial r}\Psi_0 = -2\pi r\Omega(r) \tag{A2b}$$

(see Vassilicos & Brasseur 1996). Equations (10a), (10b) and (10c) follow from (A1) and (A2).

For an inviscid Lundgren single spiral vortex sheet where $\Omega(r) = \Omega_0(r/R_0)^{-\alpha}$ and

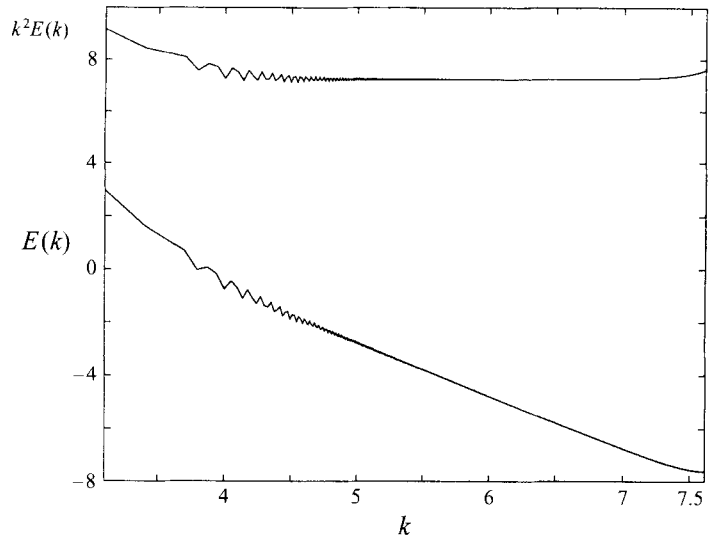

FIGURE 10. Log-log plot of the the wavenumber spectrum against the wavenumber for the Lundgren single spiral sheet vortex with $\alpha = 1$.

$f(r) = (2-\alpha)\Omega_0(r/R_0)^{-\alpha}$, equation (3.21) in Gilbert (1988) gives

$$E(k) \sim k^{-3} \sum_{n=1}^{\infty} (nt\Omega_0 R_0^{\alpha}/\pi k)^{2/(\alpha+1)} |f(r_n)|^2 \tag{A3}$$

where $r_n = (n\alpha\Omega_0 R_0^{\alpha} t/\pi k)^{1/(\alpha+1)}$ and the functions f_n in Gilbert (1988) are replaced by the single function f because we consider the case of a single spiral vortex sheet. Hence,

$$E(k) \sim k^{-3} k^{2(\alpha-1)/(\alpha+1)} \sum_{n=1}^{\infty} n^{2/(\alpha+1)} n^{-2\alpha/(\alpha+1)} \tag{A4}$$

and as explained by Gilbert (1988), the sum needs only be carried out up to $n = n_u \propto k$, so that

$$E(k) \sim k^{-3} k^{2(\alpha-1)/(\alpha+1)} \int_1^{n_u} n^{-2(\alpha-1)/(\alpha+1)}\, dn \sim k^{-2} \tag{A5}$$

for $\alpha < 3$. We also compute $E(k)$ numerically and confirm the k^{-2} form of the Lundgren single spiral vortex sheet wavenumber spectrum (figure 10).

REFERENCES

BATCHELOR, G. K. 1967 *An Introduction to Fluid Dynamics.* Cambridge University Press.

GILBERT, A. D. 1988 Spiral structures and spectra in two-dimensional turbulence. *J. Fluid Mech.* **193**, 475.

HUNT, J. C. R. & VASSILICOS, J. C. 1991 Kolmogorov's contributions to the physical and geometrical understanding of small-scale turbulence and recent developments. *Proc. R. Soc. Lond.* A **434**, 183.

INOUE, E. 1951 On turbulent diffusion in the atmosphere. *J. Met. Soc. Japan* **29**, 246.

JIMÉNEZ, J., WRAY, A. A., SAFFMAN, P. G. & ROGALLO, R. S. 1993 The structure of intense vorticity in homogeneous isotropic turbulence. *J. Fluid Mech.* **255**, 65.

LUNDGREN, T. S. 1982 Strained spiral vortex model for turbulent fine structure. *Phys. Fluids* **25**, 2193.

LUNDGREN, T. S. 1993 A small-scale turbulence model. *Phys. Fluids* A **5**, 1472.

MOFFATT, H. K. 1984 Simple topological aspects of turbulent vorticity dynamics. In *Turbulence and Chaotic Phenomena in Fluids* (ed. T. Tatsumi). Elsevier.

MOFFATT, H. K. 1993 Spiral structures in turbulent flow. In *Fractals, Wavelets and Fourier Transforms* (ed. M. Farge, J. C. R. Hunt & J. C. Vassilicos). Oxford University Press.

MOFFATT, H. K., KIDA, S. & OKHITANI, K. 1994 Stretched vortices – the sinews of turbulence; large Reynolds-number asymptotics. *J. Fluid Mech.* **259**, 241.

PULLIN, D. & SAFFMAN, P. G. 1993 On the Lundgren-Townsend model of turbulent fine scales. *Phys. Fluids* A **5**, 126.

TENNEKES, H. 1975 Eulerian and Lagrangian time microscales in isotropic turbulence. *J. Fluid Mech.* **67**, 561.

TOWNSEND, A. A. 1951 On the fine scale structure of turbulence. *Proc. R. Soc. Lond.* A **208**, 534.

VASSILICOS, J. C. & BRASSEUR, J. G. 1996 Self-similar flow structure in low Reynolds number isotropic and decaying turbulence. *Phys. Rev.* E **54**, No 1, 467.

VASSILICOS, J. C. & HUNT, J. C. R. 1991 Fractal dimensions and spectra of interfaces with application to turbulence. *Proc. R. Soc. Lond.* A **435**, 505.

VILLERMAUX, E., SIXOU, B. & GAGNE, Y. 1995 Intense vortical structures in grid-generated turbulence. *Phys. Fluids* **7**, 2008.

YEUNG, P. K., BRASSEUR, J. G. & WANG, Q. 1995 Dynamics of direct large-small scale couplings in coherently forced turbulence: concurrent physical- and Fourier-space views. *J. Fluid Mech.* **283**, 43.